

Relation of roughness parameters and tension softening diagram of concrete-to-concrete interface

A. Satoh, K. Yamada, S. Ishiyama & T. Homma
Akita Prefectural University, Yurihonjo, Akita, Japan

ABSTRACT: This paper elaborates the relation of roughness parameters and tension softening diagram of concrete-to-concrete interface. Specimens with eight types of placing joints and three types of monolithic ones were employed for the evaluation of tension softening diagram (TSD) followed by surface observations of the ligament after fracture test. Roughness parameters were measured, which include the maximum height on the fractured surfaces (Pt), with 3-dimensional roughness analyzer. The authors calculated the key factor Φ which is the ratio of fractured part excluding detached part on the surface divided by the total ligament area. The authors assumed one of the roughness parameters as a representative height of dowel, and proposed a pull-out dowel model. The dowel model can describe some important aspects which appeared in TSDs of specimens with placing joint.

1 INTRODUCTION

1.1 Concrete-to-concrete interfacial surfaces

Every concrete structure has inevitably concrete-to-concrete interfacial surfaces such as placing joint and casting of additional concrete for repair and reinforcement. In these days of heading towards rational structural design and economical construction, there are lasting needs for making the enhancement of the adhesion performance possible through complete understanding of the adhesion mechanisms, which is the main topic of this paper.

1.2 Previous studies

There are many literatures that studied the ways of enhancing the strength of placing joint experimentally, beginning at very early date (Kokubu 1950). The essence of the results is compiled for constituting many rules for placing concrete and retrofitting existing concrete structures (AIJ 2009). Though the knowledge about practical treatment for the concrete interface is prevailing, fundamental knowledge about basic mechanism of the concrete-to-concrete interface is little.

The authors have been conducting basic studies of interface of concrete, chemically and mechanically (Satoh et al. 2007, 2008a, 2008b). One of the results is that the maximum height of the fractured surface has an intimate relation with the fractured area of the surface excluding the detached part (Satoh et.al. 2008b). The mechanism producing the relation is comparable to the one between the height

of the summit and the extension area of the foot of the mountain. As is known there are some types of surface roughness parameters measurable with automated equipment other than the maximum height (JIS B 0601 2001). Relationship between these roughness parameters and mechanical performance of the interface is not known, so far.

1.3 Purpose of the research

This paper focuses on integrating the knowledge of surface roughness of concrete-to-concrete interfacial surfaces with the mechanical properties achieved by TSD (tension softening diagram) employing the latest analysis equipments.

2 EXPERIMENT

2.1 Specimens

The authors prepared eight types of specimens with varied types of placing joint made from different roughening or cured with different mold on them. Also three types of monolithic specimens with a varied size of maximum aggregate were made for a reference. Table 1 shows the attributes of specimens, and Table 2 the mix proportion of concrete.

The number of specimens was three for each case, which have a section of 100 mm by 100 mm, and a length of 400mm. After 24 hours from the 1st cast of concrete in the half part of mold, the joint surface was roughened in the case of R. Then concrete was cast in the remained half of mold as de-

pictured in Figure 1. The specimens were cured in water at 20°C for 28 days after the final cast of concrete. A 50mm depth notch was incised at the center of the specimen before the fracture toughness test.

Table 1. Attributes of specimens.

Specimen	Surface condition
N	Monolithic, Max. aggregate size : 20 (mm)
N950	WS*1, Max. aggregate size : 9.5 (mm)
N236	WS*1, Max. aggregate size : 2.36 (mm)
J	Joint sheet
E	Exposed aggregate
R	Roughened with steel wire brush
SP	As-cast with steel plate
PW	As-cast with painted ply wood
A	As-cast with acrylic resin board
G	Sheet glass remained
FS-3528	Fractured surface

*1: Wet screening was done.

Table 2. Mix proportion of concrete.

W/C (%)	s/a (%)	Weight of materials (kg/m ³)				
		Water	Cement	Sand	Gravel	Ad
51.4	43.0	177	344	739	1010	1.72

Ad: Super plasticizer

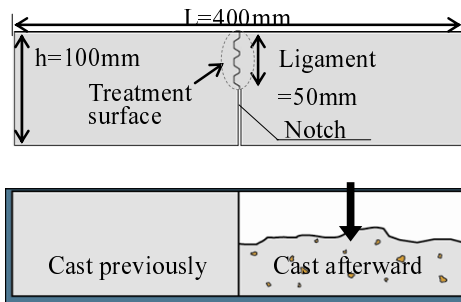


Figure 1. Typical detail of specimen (top) and method for producing specimen (bottom).

2.2 Tension softening diagram

Fracture toughness test was executed with observing RILEM's recommendation (RILEM 1985). Load and crack mouth opening displacement (CMOD) were measured continuously during the loading. To cancel the dead weight of specimen and to obtain a good and precise measurement, a counter weight made of steel was glued at each end of specimens. Servo type loading equipment was used to get high-speed response with the help of feed-back system of the equipment.

TSD was achieved from the load-CMOD curve of specimen with employing multi-linear approximation method which was standardized by JCI (JCI 2004). Fracture energy is consumed energy during the fracture of a ligament and displayed as an area enclosed with x-axis, y-axis and TSD in the graph, which is abbreviated as GF. The f_t is tension softening initial stress which is the same as tensile strength,

and W_{cr} is a crack width when load becomes zero (critical crack width).

2.3 Observations with analyzing equipments

After fracture toughness test, fractured area in ligament was observed to detect characters of interfaces. At first, the surface of fractured ligament was observed with laser 3-D measuring machine at two levels of interval; 200 μ m and 1 μ m. Figure 2 depicts a typical example of the roughness parameters from measured 3-D data which was standardized by JIS B 0601 (JIS B 0601 2001). From the measurement where reference length (L_r) was 100mm (for 200 μ m interval) or 5mm (for 1 μ m interval), the data were processed at three conditions, where cut off values of wavelength (λ_c) are 0.25mm, 0.80mm and 2.5mm. The roughness parameters were evaluated within an above-mentioned certain wavelength where the wave height due to undulation was excluded. (Fig. 2) The undulation is the long wave which exceeds the certain wavelength.

The authors cut a sample of 1 cm square from the surface of each specimen. After platinum sputtering on it, SEM (scanning electron microscope) observation was done. In addition, the sample was placed edgewise between slide glasses in resin. Quantitative analysis of Ca and Si were done with using EPMA (Electron probe micro analyzer).

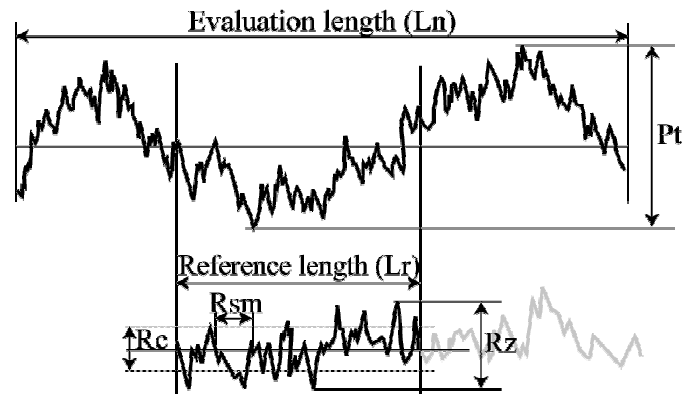


Figure 2. Typical roughness parameters of surfaces.

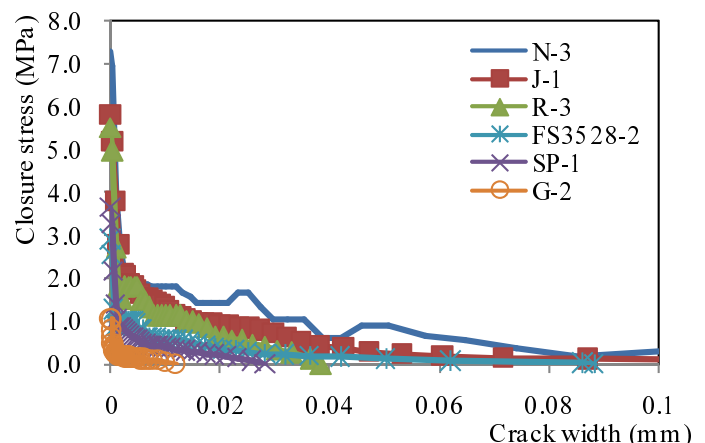


Figure 3. Tension softening diagrams of specimens.

Table 3. Mechanical properties of specimens.

Specimen	fb (MPa)	ft (MPa)	GF (N/mm)	Wcr (mm)
N-3	4.60	7.28	0.1160	0.2243
N950-2	3.66	4.70	0.0642	0.1769
N236-2	3.24	3.03	0.0331	0.0400
J-3	3.53	4.76	0.0501	0.1174
E-3	2.80	3.26	0.0372	0.0835
R-2	3.03	5.68	0.0296	0.0507
SP-1	2.00	3.65	0.0112	0.0282
PW-3	3.28	3.77	0.0543	0.1267
A-3	2.51	2.74	0.0148	0.0292
G-2	0.69	1.03	0.0015	0.0119
FS-3528-3	2.11	2.11	0.0288	0.1054

3 RESULTS

3.1 Resulted mechanical properties

Figure 3 and Table 3 show achieved TSDs and the mechanical properties of specimens respectively. The resulted GFs are ranging from 0.002N/mm (specimen G) to 0.05 N/mm (specimen J) with a reference result of 0.1N/mm for specimen N. Compressive strength is 42.7 MPa.

3.2 Roughness parameters

The authors classified the surface of fractured ligament in two types after fracture toughness test. One is a fractured part and the other is a detached part, which are described black part and white part in Figure 4 respectively. The fractured part was characterized by exposed aggregates or rough part where the height is greater than 0.2mm. Figure 5 shows distribution of height on the fractured surfaces at the center of the ligament which were measured at 200 μm intervals with laser 3-D measuring machine.

Figure 6 represents relationship between Pt and Φ, where Φ is a ratio of fractured part excluding detached part on the surface divided by the total ligament area, and Pt is the maximum height on the fractured surface within the measured region. The graph tells that there is a correlation between Pt and Φ. We can also observe that the value Φ is different from each other

influenced by the conditions of treatment of the joint.

The parts of fractured ligament were classified into five types, which are from (A) to (E) in Table 4. Type (A) is the flattest surface of detached part like the surface of specimen-G. Type (B) is interfacial transient zone (ITZ) on the surface of aggregate. Type (C) is detached part of specimens of placing joint other than specimen-G. Type (D) is fractured surfaces excluding ITZ of joint specimens and (E) is that of monolithic one. The data in Table 4 are the average values measured at 1 μm intervals with laser 3-D measuring machine.

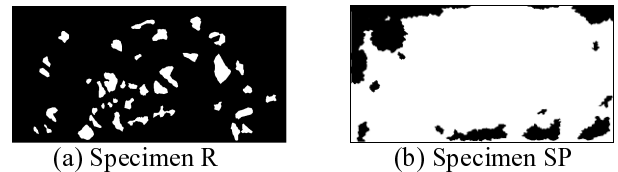


Figure 4. Samples of classified ligaments into fractured part (black) and detached one (white).

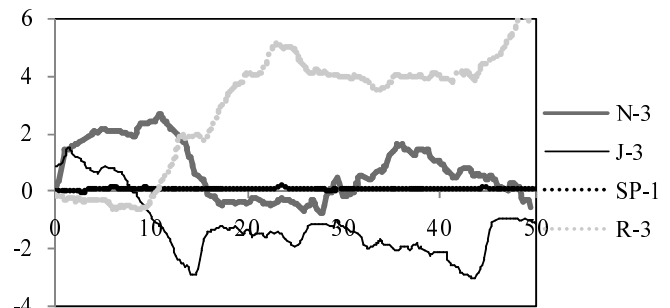


Figure 5. Distribution of height on the fractured surfaces.

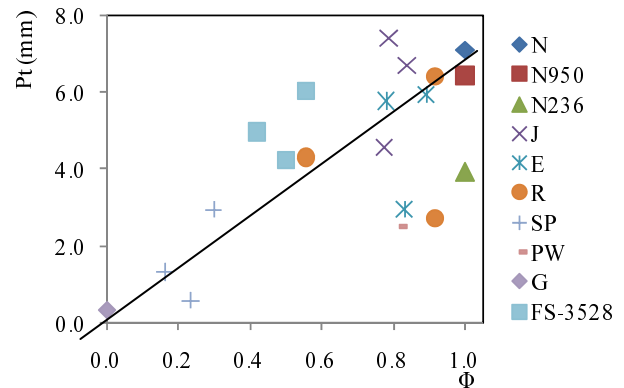


Figure 6. Relationship between Φ and Pt.

Table 4. Features of roughness parameters in typically classified surfaces.

Parameters	unit	standard length and cut off value (λc) = 0.25mm								
		(A)	(B)	(C)	(D)	(E)	B/A	B/C	D/C	E/D
maximum height (Rz)	μm	13.02	29.30	19.85	38.14	37.87	2.250	1.475	1.921	0.993
average height (Rc)	μm	6.30	16.66	10.36	22.06	23.69	2.644	1.609	2.130	1.074
average wavelength (RSm)	μm	15.95	52.06	37.27	58.84	67.71	3.264	1.397	1.579	1.151
Parameters	unit	standard length and cut off value (λc) = 0.80mm								
		(A)	(B)	(C)	(D)	(E)	B/A	B/C	D/C	E/D
maximum height (Rz)	μm	27.94	59.46	34.58	101.6	96.83	2.128	1.720	2.937	0.953
average height (Rc)	μm	12.90	34.60	18.30	63.37	53.21	2.682	1.891	3.463	0.840
average wavelength (RSm)	μm	86.73	153.5	89.13	221.4	240.0	1.770	1.722	2.485	1.084
Parameters	unit	standard length and cut off value (λc) = 2.50mm								
		(A)	(B)	(C)	(D)	(E)	B/A	B/C	D/C	E/D
maximum height (Rz)	μm	24.89	123.8	37.18	290.4	235.6	4.975	3.330	7.809	0.811
average height (Rc)	μm	12.89	59.10	16.85	140.1	118.3	4.586	3.507	8.312	0.845
average wavelength (RSm)	μm	88.33	422.5	181.0	707.5	649.9	4.783	2.334	3.909	0.919

In Table 4, one can naturally realize that the average height (R_c) on detached parts ((A) - (C)) is lower than the one on fractured parts ((D), (E)). It is worthy to note that even in the case of (A), which is the surface of joint made with sheet glass mold and is considered to be almost flat, the roughness (R_c) is $6.3\mu\text{m}$ (reference length is 0.25mm).

The value B/C for R_c and R_z in the table is about 1.5 (in the case that λ_c is 0.25mm and 0.8mm) telling that the roughness is 1.5 times larger in the case of (B) than the one in the case of (C) even for the same detached parts. It may suggest that the part (B), which is ITZ around coarse aggregates, can contribute to mechanical performance even higher than part (C). Then the detached part (C) may be smoother than ITZ, where insufficient adhesion may have occurred.

On the other hand, if we compare the roughness parameters of both fractured parts (D) and (E), we can see that R_c and R_z are almost the same as the value E/D is almost 1.0 in all cases of λ_c (from 0.25mm to 2.5mm). This fact is important because it is related to the previous study (Sato et. al. 2008b) which told that fractured part in the ligament contributed to fracture energy (GF) at the same rate as monolithic one regardless of the joint types.

Interesting finding is that, while R_c and R_z of both detached and fractured parts are getting larger along with λ_c , the tendency of the growing rates of them are different. It means that the growing rate (in all cases of λ_c) of R_c for detached part is about 2.0, whereas the one for fractured part is over 5.0, suggesting the effect of undulation is dominant at the fractured part compared to the detached part.

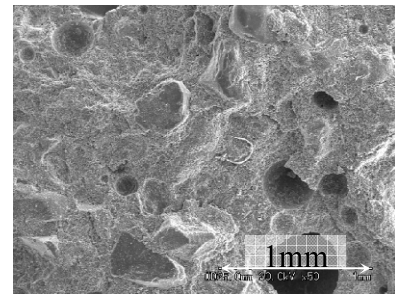
3.3 Observations by SEM and EPMA

Figure 7(a) shows the SEM photo of a sample from specimen-N, where one can observe a rough surface and many fine aggregates half-embedded in it. In the case of specimen-G (Fig. 7(b)), one can observe smooth membrane mainly made of $\text{Ca}(\text{OH})_2$.

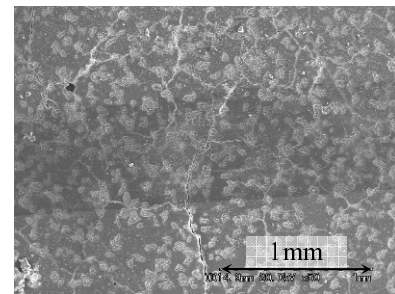
Figure 8 depicts Ca/Si map which the authors composed for analyzing the difference of phases from constituent concrete (Sato et. al. 2008a). The map shows three colors representing the graded mass ratio of Ca divided by Si from the results of quantitative analysis of Ca and Si with EPMA. In the map, gray zone represents CSH gel where the ratio is between 1.0 and 3.0, black zone represents $\text{Ca}(\text{OH})_2$ where the ratio is over 3.0, and white zone represents aggregates mainly consists of SiO_2 or porosity where the ratio is below 1.0.

In Figure 8, we can find specific distribution of $\text{Ca}(\text{OH})_2$. The detached part of specimen-A, -G has thick black layers, meaning that these ones are made of $\text{Ca}(\text{OH})_2$. Fractured surface of specimen-R has no such black layer, though Ca/Si is high around some aggregates in Figure 8(c). In this map, almost all of

the parts can be assumed to be CSH gel, because the gray zone is abundant telling the effects of roughing. It can be said that the Ca/Si map reveals the weak layer of $\text{Ca}(\text{OH})_2$ which plays a primary role on the crack path.

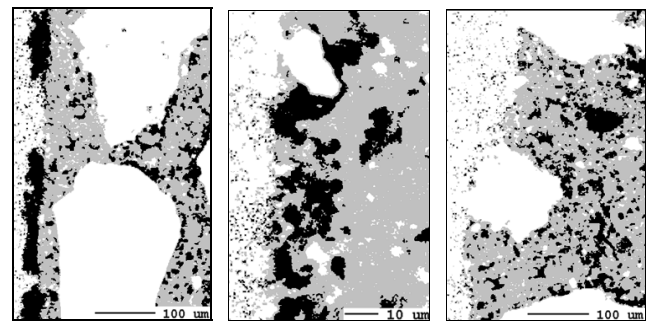


(a) Fractured surface of specimen-N



(b) Detached surface of specimen-G

Figure 7. SEM Observations on the surfaces.



(a) specimen-A (b) specimen-G (c) specimen-R

Figure 8. Ca/Si maps from the side of the interface.

4 DISCUSSION

4.1 Influence of fine aggregate on fractured surface

The authors propose a model depicted in Figure 9, where fine aggregates are assumed to be spheres whose diameter is l_c (l_c is likened to fiber length), based on the SEM photo (Fig. 7(a)).

Given there is some thin layer of cement paste around aggregate by a wall effect, aggregates are modeled to line at the same interval. The projection length of the aggregate is assumed to be $l_c/4$ which is analogues to the average fiber length in fiber reinforcement theory. Then, after fracture, there appears a fractured surface that looks like the one depicted in Figure 9.

The term (D) in Table 4 tells R_{sm} is about $700\mu\text{m}$ when λ_c is 2.5mm , then the diameter of aggregate is calculated to be 0.39mm and R_c is to be $194\mu\text{m}$ based on the relationship depicted in Figure

9. This result (194 μm) is the medium value of Rz and Rc in Table 4. The same relationship is observed when λc is 0.8 mm (where Rsm is 220 μm), the size of aggregate is calculated to be 0.12mm and Rc is to be 61 μm , which are consistent values with the model predicted in Figure 9. Moreover, even when λc is 0.25mm which is very small region compared to the ordinarily imagined aggregate size, the consistency of the model is recognized; i.e. as Rsm is 60 μm , the aggregate size is 40 μm , and then Rc is 18 μm . Though we can see small fine aggregate (about 100 μm or smaller) in Figure 7, the model is consistent within a certain region..

From the aggregate size and mix proportion used in the study, the numbers of aggregates can be calculated. The numbers of aggregates in a certain volume where one piece of maximum size aggregate (20mm) occupies are vast (6,000pcs. for 0.6mm, 230,000pcs. for 0.3mm and 1,000,000pcs. for 0.15mm and below 0.15mm). These numbers are realistic from the observation in Figure 7 and Figure 8. As the surface roughness is deeply related to the mechanical performance (Sato et. al. 2008b), the importance of very small-sized fine aggregate should be emphasized.

On the contrary, in the case of detached part and ITZ, the dependency of roughness on λc is not clear. For example, Rc of (A) and (C) in Table 4 is smaller when λc is 2.5 than when λc is 0.25. The calculated aggregate size is 40 μm or smaller on the detached surfaces based on the same model depicted in Figure 9. These 'small aggregate' may not be aggregate but some kind of mixture of $\text{Ca}(\text{OH})_2$ and aggregate from the observation in Figure 8(b).

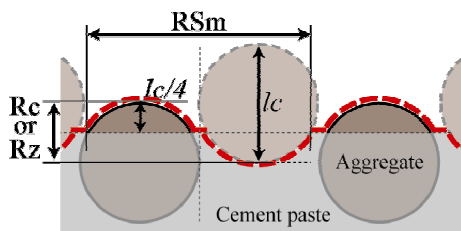


Figure 9. Model for determining relation between aggregate size and roughness parameters.

4.2 Pull-out dowel model

The above mentioned model can be easily evolved to tensile dowel model which the authors proposed in the literature (Sato et. al. 2009). In this model, extracting stress against crack propagation after cracking is only made by many sizes of aggregates. The aggregates act as dowels which have different lengths. Before cracking, the tensile strength of the interface is determined by the ratio of composition of $\text{Ca}(\text{OH})_2$ and CSH. (Fig. 8)

In Figure 10, the fat and short fiber (dowel) is a model of a given size of aggregate. Assuming that the

extracting force of dowel follows the fiber reinforcement theory which Naaman proposed (Naaman 1989), following Equation are lead. The Naaman Model describes a relationship between extracting force and extracted displacement for steel fiber, as follows.

$$P_c = \frac{t_{\max}}{\lambda} \frac{(1 - e^{-2\lambda l})}{(1 - V_f)(1 + e^{-2\lambda l}) + 2V_f e^{-\lambda l}} \quad (1)$$

$$\Delta_c = \frac{P_c \xi}{\lambda} \frac{(1 - e^{-\lambda l})}{(1 + e^{-\lambda l})} \quad (2)$$

where, P_c is the maximum extracting force, Δ_c is the displacement at P_c , V_f is the ratio of area of fiber divided by the total area, t_{\max} is the shearing force per length supported by a dowel (the multiplied value of τ_{\max} (interfacial shearing stress) and circumference length ψ) and l is the embedded length. The constant λ is determined by the extracting rigidity k , which is the shearing stress per unit displacement.

The Equation (1) and (2) are the results for a single fiber. Then the extracting force for multiple fibers is described in equation (3).

$$P_A = \sum_l N(l) P_c(l) \quad (3)$$

where, $P_c(l)$ is P_c for the given length l and $N(l)$ is the numbers of the fiber of given length l .

The numbers of dowel is linked to that of aggregate in this model. Then, if the volume of aggregate of each size is the same, $N(l)$ is proportional to the value l^3 . Naturally $P_c(l)$ is the cross section area of the fiber which is proportional to the value l^2 . Then finally P_A is proportional to the value l^1 .

Figure 12(a) shows the load-displacement relationship of the dowel whose length is l or $2l$ based on above mentioned model. In the figure, PMA represents the strength of weak matrix and PMB is the strength of the strong matrix. As is discussed in previous study (Sato et al. 2009) which is displayed in Figure 11, the strength of interface and the depth of FPZ have close relationship. If the depth of FPZ of matrix (A) is shallow, the depth of fractured matrix tends to be shallow in which short dowels are included. On the contrary, if the depth of FPZ of matrix (B) is deep, the depth of fractured matrix tends to be deep in which long dowels are included. This model clearly shows the morphological feature of TSD as is depicted in Figure 12(b). Moreover, the deep FPZ tends to fracture wide region of matrix which makes the fracture surface wide, then making Φ large.

The model also expresses the reason why Φ is related to tensile strength f_t in TSD. The reason for it is as follows. Tensile strength f_t is the sum of

strength of matrix and extraction force of dowel. At the same time, both strength of matrix and the length of dowel are related to Φ as we discussed above. Then Φ is related to tensile strength f_t .

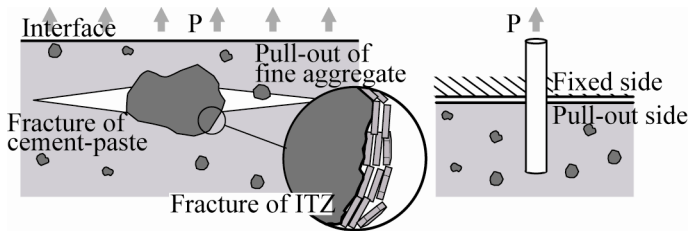


Figure 10. Modeled dowel from aggregate.

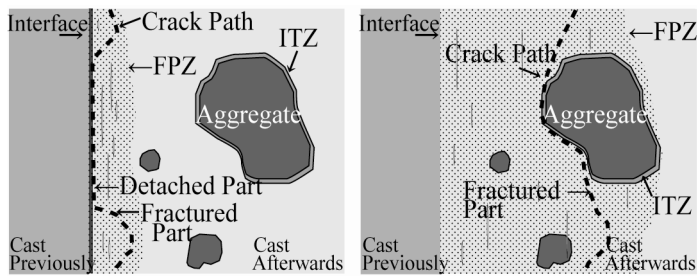
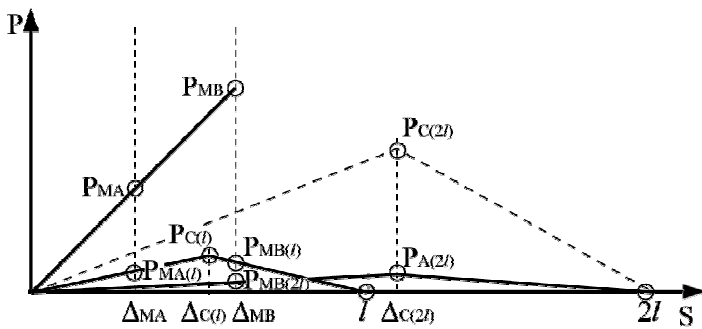
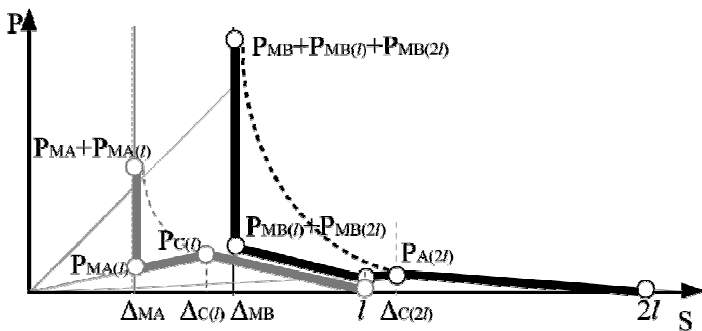


Figure 11. Fracture region and depth influenced by the strength of interface property: weak interface (left picture) and strong one (right picture).



(a) Tensile force of matrix and extraction force of dowel



(b) Combined force of matrix and dowel

Figure 12. Relationship between TSD and dowel model.

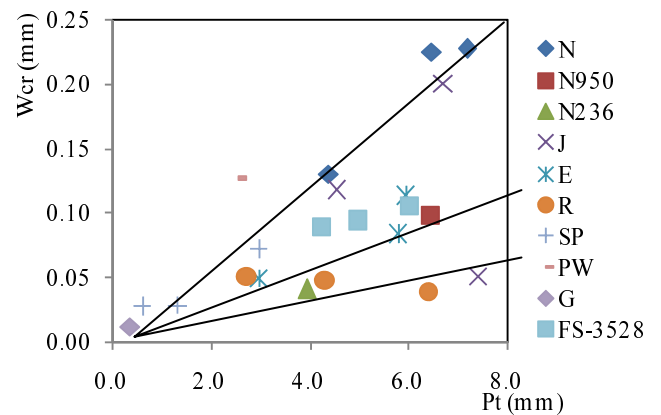
The model also describes the reason why aggregate influences W_{cr} in TSD. The reason for it is as follows. The strong interface which has high f_t fractures the wide region where long dowels (large aggregate) are included, which leads to large critical width W_{cr} in TSD, whereas weak interface which has low f_t fractures the narrow region where short dowels (small aggregate) are included, which leads to small W_{cr} . So, strong interface brings both high f_t

and large W_{cr} together resulting high fracture energy GF, because GF is influenced by both f_t and W_{cr} .

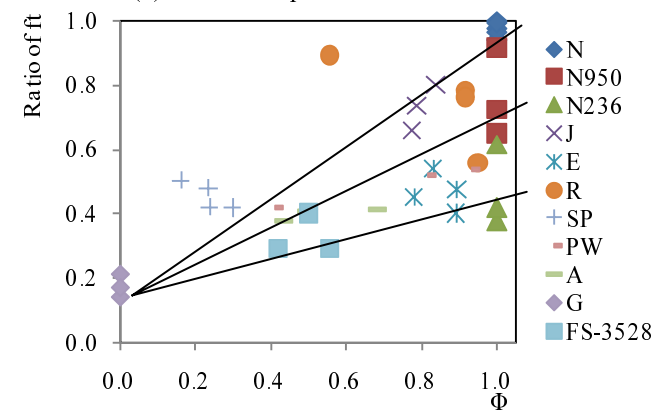
4.3 Relationship between mechanical performance and roughness parameters

The relationship between mechanical properties and roughness parameters of fracture surface is depicted in Figure 13(a)-(c).

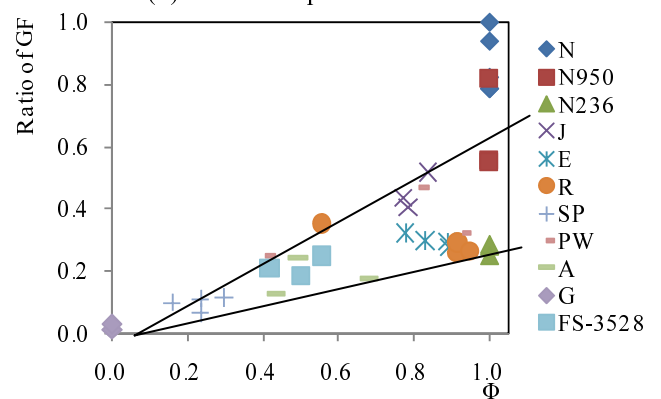
The relationship between W_{cr} and P_t in Figure 13(a) reflects the size of maximum aggregate, which is natural because P_t is linked to the length of dowels. As Figure 6 showed, P_t and Φ are closely related. This is also natural, because P_t is comparable to 'height of mountain' whereas Φ is comparable to 'range of the foot of the mountain'.



(a) Relationship between P_t and W_{cr}



(b) Relationship between Φ and f_t



(c) Relationship between Φ and GF

Figure 13. Relationships between roughness parameter and mechanical property.

After all, Φ is closely related to Pt. It is surely supposed that Pt is closely related to Rc and Rz from the well known fact that concrete has a nature of fractal characteristics on its fractured surface (Mihashi 1993). Then these four parameters (Φ , Pt, Rc and Rz) have the same root: i.e. dowel action.

Figure 13(b) represents the relationship between Φ and ft, which shows that ft is basically determined by Φ . But even detached part produces ft which originates from chemical adhesion, which produces some ft in specimen-G whose Φ is zero.

As GF is the enclosed area within TSD, x-axis and y-axis, then GF is strongly affected by ft and Wcr. So, finally GF and Φ are proportional as Figure 13(c) shows. Then if Φ grows, GF also grows.

5 CONCLUSIONS

The authors conducted fracture mechanics test of eight different types of concrete prisms which have a vertical placing joint in them, and three types of monolithic ones which have different size of aggregate.

The findings are as follows.

1. There are three typical values of roughness parameters for fractured part, detached part and interfacial transition zone.
2. Dowel model was proposed which can be used to discuss the relationship between roughness parameters and morphological feature of TSD.
3. The mechanism which governs relationship between roughness parameters (Rc, Rz, Pt) and mechanical properties (ft, GF, Wcr) is revealed.

ACKNOWLEDGEMENTS

This study was financially supported by 'Grant-in-aid for JSPS fellows (Grant No. 21-10339 for DC-1)' by JSPS, which the authors gratefully acknowledge.

REFERENCES

- AIJ. 2009. *Japanese architectural standard specification, Reinforced concrete work, JASS 5*. Tokyo: AIJ.
- JCI. 2004. Test method for fracture energy of plain concrete (Draft). In Izumi, I. (ed.), *JCI standards*. Tokyo: JCI.
- JIS B 0601. 2001. *Geometrical Product Specifications (GPS) - Surface texture: Profile method- Terms, definitions and surface texture parameters*. Tokyo: JIS.
- Kokubu, M. 1950. A study on placing joint between old and new concrete. *Trans. JSCE*: 8, 1-24.
- Mihashi, H., Umeoka, S. & Miura, S. 1993. Fundamental study on analysis of fractured surface of cementitious materials. *Trans. AIJ*: 445, 19-25.
- Naaman, A.E., Namur, G., Najm, H. & Alwan, J. 1989. Bond Mechanisms in Fiber Reinforced Cement Based Composites, *Report No. UMCE 89-9*, Ann Arbor: Dept. Civil Eng., Univ. Mich.
- RILEM. 1985. Draft Recommendation, Determination of the Fracture Energy of Mortar and Concrete by Means of Three-point bend Tests on Notched Beams. *Mat. & Struct.*: 18(106) 285-290.
- Satoh, A., Yamada, K. & Ishiyama, S. 2007. A Discussion on Tension Softening Characteristics and Fracture Process of Concrete Prism with a Vertical Placing Joint. *Proc. AIJ Tohoku chap.*: 70, 49-55.
- Satoh, A., Yamada, K. & Ishiyama, S. 2008a. Fractographic Discussion on Vertical Construction Joints Cast with Form of Different Material in Concrete Prism. *Proc. AIJ Tohoku chap.*: 71, 1-8.
- Satoh, A., Yamada, K., & Ishiyama, S. 2008b. A Discussion on Fracture Energy of Vertical Joint in Concrete. *Proc. 17 Eur. Conf. Frac.*: 1530-1537.
- Satoh, A., Yamada, K. & Ishiyama, S. 2009. Discussion on relationship between strength and ductility of interface between new and old concrete employing tension-softening-diagram and pull-out dowel model. *Trans. AIJ*: 74(637) 417-424.